Proceedings of ASME FEDSM'00
ASME 2000 Fluids Engineering Division Summer Meeting
June 11-15, 2000, Boston, Massachusetts

FEDSM2000-11255

NUMERICAL SIMULATION OF FREE-SURFACE FLOWS USING A MOVING UNSTRUCTURED MESH

Ramesh Nallapati, Blair J. Perot
Department of Mechanical and Industrial Engineering, University of Massachusetts, Amherst, Amherst, MA 01003.

Abstract

A new moving mesh approach is used for numerical simulation of incompressible flow problems involving free-surfaces. The divergence form of the Navier-Stokes equation is discretized using an unstructured staggered mesh method. This method exploits the inherent advantages of the Delaunay-Veronoi co-volumes, which exhibit an orthogonal behavior. The paper also describes the semi-Lagrangian mesh adaptive technique used to track the free-surface. Results obtained from implementing this numerical technique on a few free-surfaces flows are presented and discussed.

1. Introduction

The study of free-surface flows covers a wide range of engineering and environmental flows, including such areas as small-scale bubble dynamics, wave mechanics, flow about a ship or offshore structure, open-channel flows and ocean-atmosphere interactions. The phenomena we consider often happen on scales of space and time where experimental visualization is difficult or impossible. In such cases, numerical simulation may bring useful insight to the physicist or the engineer.

The presence of free-surfaces poses a very interesting and challenging numerical problem in that, the location of the free-surface and hence the shape of the domain of interest may be time dependent. Tracking the free-surface is critical to accurate solution of such problems. In the present work, a new moving mesh approach with discretization based on an unstructured staggered grid is used to track the free-surface.

2. The unstructured staggered mesh approach

The approach adopted in the current work is a generalization of a particular staggering scheme that dates originally to the work of Harlow and Welch [1]. They describe a scheme for regular Cartesian meshes where the pressure is located at cell centers but the velocity is distributed on the cell faces with horizontal velocity components prescribed at vertical faces and vertical velocity components prescribed at horizontal faces. This particular staggering scheme has been found to be especially attractive for simulations of incompressible flow and is widely used for this class of flows. The important property for incompressible flows is the fact that this scheme does not display spurious pressure modes. There is no red-black uncoupling of the pressure unknowns or a need for 'stabilization' terms that damp pressure and velocity fluctuations. Several properties beyond the ability to easily simulate incompressible flow make this method attractive for simulations of high Reynolds number flows. The method is typically very fast and uses minimal memory.

The staggered mesh method of Harlow & Welch was generalized to unstructured (triangular) meshes independently by Hall, Peterson, Porshing & Sledge [2] and by Nicolaides [3-5]. The works of Nicolaides provide extensive mathematical analysis of the method. These 'dual mesh' or 'covolume' methods take explicit advantage of the fact that every unstructured tetrahedral or triangular mesh (a Delaunay mesh) has an orthogonal or dual mesh associated with it (a Voronoi tessellation). An example of an unstructured mesh and its dual

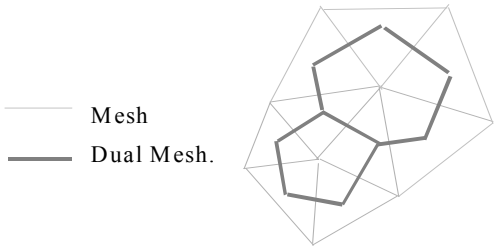

Figure 1. Example of two-dimensional unstructured triangular mesh and the associated Veronoi dual mesh. The faces of the two meshes are always locally orthogonal. The locally orthogonal dual mesh concept can be generalized to three-dimensions (and higher).

are shown in fig. 1. The local mutual orthogonality of these meshes can be used to develop discretization operators that closely mimic their continuous counterparts. This allows a true inner product to be defined and important vector identities (such as $\nabla \cdot \nabla \times (\bullet) = 0$) to be maintained in a discrete sense.

3. Governing equations:

Different discretizations of the Navier-Stokes equations are possible depending on which form of the equations are discretized. In this work, the divergence form of the Navier Stokes equations for incompressible flow are used for discretization and are presented below:

Conservation of mass: $$\nabla \bullet \mathbf{u} = 0 \qquad (1)$$

Conservation of momentum:

$$\frac{\partial \mathbf{u}}{\partial t} + \nabla \bullet (\mathbf{u}(\mathbf{u} - \mathbf{v})) = -\nabla p + \nabla \bullet \nu(\nabla \mathbf{u} + \nabla \mathbf{u}^{T}) \qquad (2)$$

where **u** is the velocity of the fluid and **v** is the velocity of the control surface**.** Discretizations based on the divergence form of the equations are of interest because they are able to discretely conserve momentum. While momentum conservation is a trivial consequence of a classical finite volume method, it is not an obvious trait of staggered mesh methods. This is because the staggered mesh methods only update the normal velocity components at cell faces, while the tangential velocity components are interpolated, but not evolved. It is shown that with certain choices of the interpolation operators, the staggered mesh update of face normal velocities is directly equivalent to a classic finite volume method which updates the velocity vector at cell centers. [6]

4. Discretization of the equations:

4.1 Mesh configuration: Pressure and velocity, the two independent variables of the problem, are located in a staggered manner as shown in fig. 2. The normal velocity U at each face is assumed to point from cell C1 to cell C2 and pressure P is located at the cell circumcenters. At boundary faces the normal vector is assumed to point out of the domain and cell C2 is a virtual cell located at the domain boundary.

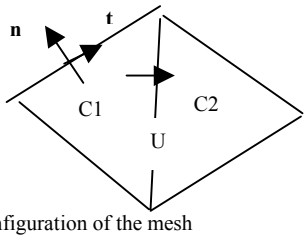

Figure 2 : Configuration of the mesh

4.2 Conservation of mass: This equation is satisfied automatically by the definition of the normal velocity at each face, which is computed as the discrete curl of stream function.

4.3 Conservation of momentum: The divergence form of the Navier-Stokes equation is discretized to obtain an evolution equation for the normal face velocity component and is given by,

$$W_f A_f \frac{u^{n+1} - u^n}{\Delta t} + \mathbf{n}_f \cdot (W_{C1}^f \mathbf{c}_{c1} + W_{C2}^f \mathbf{c}_{c2}) A_f = -(p_{c2} - p_{c1}) A_f + \mathbf{n}_f \cdot (W_{C1}^f \mathbf{d}_{c1} + W_{C2}^f \mathbf{d}_{c2}) A_f \qquad (3)$$

where $\mathbf{c}_c = \frac{1}{V_c} \sum_{\substack{cell \\ faces}} \mathbf{u}_f (\hat{u} - \hat{v}) A_f$ is a conservative discretization of the convection term evaluated in each cell, $\mathbf{d}_c = \frac{1}{V_c} \sum_{\substack{cell \\ faces}} \nu(\nabla \mathbf{u} + \nabla \mathbf{u}^{T}) \cdot \hat{\mathbf{n}}_f A_f$ is a conservative discretization of the diffusion term evaluated in each cell, V_c is the volume of each cell, A_f is the face area, W_f is the distance between neighboring cell circumcenters, and W_C^f is the distance between the face circumcenter and the cell circumcenter. Note that $u = \mathbf{u} \cdot \mathbf{n}_f$ is the normal velocity component at each cell face and $\hat{v}$ is the normal velocity component of the mesh. Similarly $\hat{\mathbf{n}}_f$ is the normal vector pointing out of a particular cell. It has been shown by Perot[7] that such discretization conserves both momentum and kinetic energy.

The convection and diffusion terms in the above expression require the velocity vectors at the cell positions to be evaluated. The following interpolation scheme is used for computing the cell velocity from face-normal velocities:

$$\mathbf{u} V_c = \sum_{\substack{cell \\ faces}} \hat{u} \mathbf{r}_f^{CC} A_f \qquad (4)$$

where V_c is the volume of the cell under consideration, $\hat{u}$ is the outwards normal component of the velocity at the cell faces and $\mathbf{r}_f^{CC} = (\mathbf{x}_f^{CC} - \mathbf{x}_c^{CC}) = \hat{\mathbf{n}}_f D_{ef}$. $\mathbf{x}_f^{CC}$ and $\mathbf{x}_c^{CC}$ are face and cell circumcenter positions respectively, while D_{ef} is the distance between the face and cell circumcenters. This is a first order approximation relating the cell velocity vector to the normal velocity components at the faces. For a more detailed analysis of this interpolation scheme, the reader is recommended to refer to the work of Perot[7].

The pressure term in eq (3) in the interior cells is eliminated by performing a curl operation on the entire set of discrete equations. However, pressure needs to be introduced

along with surface tension as a boundary condition, as shall be explained in more detail in the following section.

5. Free-surface boundary condition:

A constant pressure boundary condition is used for the free-surface. Surface tension is treated as an additional term in pressure. Mathematically, pressure is evaluated as follows:

$$p = p_0 + \frac{\sigma}{R_{effective}} \qquad (5)$$

where $$\frac{1}{R_{effective}} = -\mathbf{n} \bullet \nabla^2 \mathbf{h}(x, y) \qquad (6)$$

Here, P_0 is the external pressure, σ is the surface tension coefficient, $R_{effective}$ is the effective local radius of curvature, **n** the unit normal vector while **h** is the position vector of the free-surface.

6. Free-surface tracking method:

In the present method, a new adaptive mesh approach is used that tracks the free-surface in a mixed manner between the Lagrangian motion and the fixed Eulerian point of view. The mesh at the free-surface moves in a Lagrangian manner, tracking the free-surface and exactly preserving the fluid volume. The mesh in the interior does not move with the fluid. It moves in a manner so as to achieve high quality cell shapes and connectivity. Some of the adaptive mesh features are described in detail below:

6.1 Mesh smoothing: As the mesh-nodes on the free-surface boundary move with velocity equal to that of the fluid in a *Lagrangian* manner, the internal cells get distorted and may lose useful properties that are associated with smooth, acute angled cells. To retain high quality cell shapes, a smoothing technique is implemented. This technique essentially treats each cell face as a spring under tension with the other cell-faces sharing the same node. (see fig 3). The spring restoring force is chosen proportional to the area of the face, implying, faces with larger areas tend to pull their adjoining nodes closer to themselves. The resulting forces at the nodes are computed and the positions of internal nodes are rearranged through an iterative scheme until the nodes attain a state of equilibrium.

6.2 Mesh flipper: As discussed earlier, distortions in the cell shapes could result in the loss of Delaunay properties of the cells which are very important for accurate results. To overcome this problem, a mesh-flipper is implemented, which detects non-Delaunay faces and flips them between the two neighboring cells to restore Delaunay properties as shown in fig. 4.

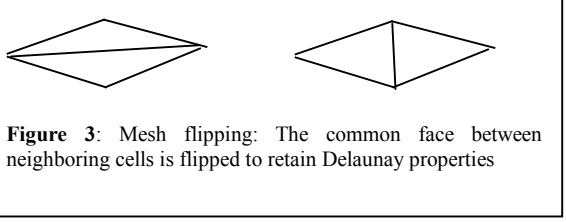

Figure 3: Mesh flipping: The common face between neighboring cells is flipped to retain Delaunay properties

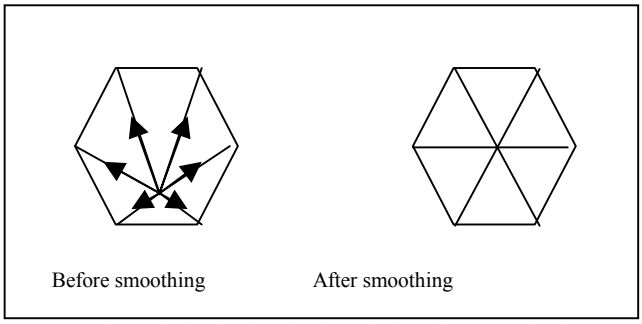

Figure 4: The node in the interior is pulled to the center by the smoothing algorithm

The smoothing and flipping functions can be extended to three dimensions in a similar fashion. Although the smoothing function in 3D is just an extension of its 2D counterpart, flipping in 3D is a little more complicated as it involves flipping of 2 or 3 tetrahedra simultaneously to produce 3 or 2 new tetrahedra respectively. Joe[8] discusses the details of 3D flipping in more detail.

7. Results and discussion:

This section presents results obtained from the numerical simulation of some free-surface flows using the present adaptive mesh method.

7.1 *Validation of the code:* The problem we considered for validating the code consists of standing waves in a rectangular tank with sufficiently small displacement. The results from the code are compared with the analytical solution for gravity induced standing waves in an irrotational fluid contained in a two-dimensional rectangular tank. It is easy to show that the fundamental period of sloshing of standing waves with a wave-length λ in a rectangular container of initial depth *D* is given by[9]:

$$T = \frac{1}{\left[\frac{g}{2\pi\lambda}\tanh\left(\frac{2\pi D}{\lambda}\right)\right]^{\frac{1}{2}}} \qquad (7)$$

In the numerical model to the present problem, the fluid is assumed to be inviscid and incompressible. The wavelength of the standing waves is taken to be twice the width of the tank. As an initial condition, the shape of the free-surface is assumed to be a sinusoidal wave and the fluid is assumed to be at rest. The unsteady potential flow equations are then solved and the results are compared with the analytical solutions.

Table 1 presents the comparison of numerical and analytical solutions for various values of gravity. It is clear that the results from numerical simulation are in good agreement with the analytical solution.

	Gravity ms^{-2}	Time period (s)		% error
		Analytical	Numerical	
1	4.90	16.0440	15.8776	1.04
2	9.80	11.3499	11.2394	0.97
3	20.0	7.9410	7.85705	1.06

Table 1: Comparison of analytical and numerical results for the standing wave problem

7.2 Some numerical examples:

In this section, numerical solutions of a few problems are presented : sloshing of a viscous fluid in a rectangular tank, axi-symmetric sloshing in a cylindrical tank and impingement of a cylindrical droplet onto a wall.

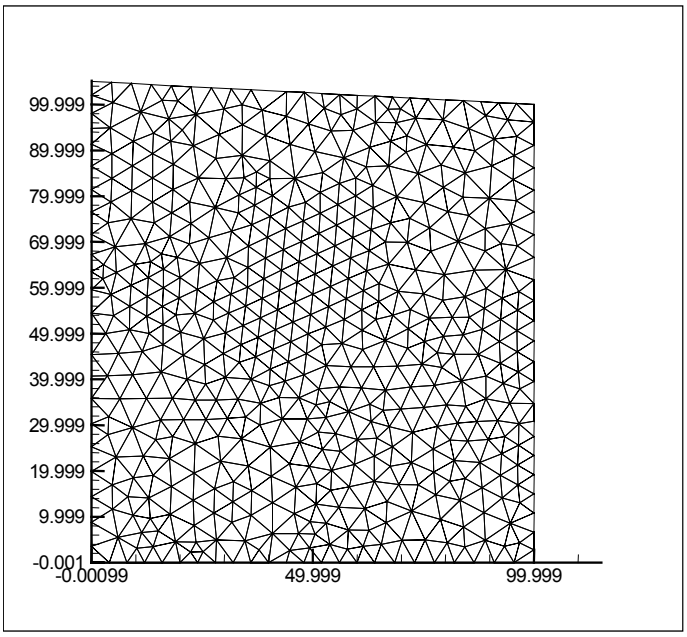

Figure 5(a): Initial state of the free surface

7.*2.1 Sloshing of a viscous fluid in a rectangular tank:* Viscous sloshing of an incompressible fluid contained in a two-dimensional rectangular tank is simulated. The free-surface is assumed to be at rest with a linear, slanted surface as an initial condition. The maximum Reynolds number in the problem is found to be approximately 100.

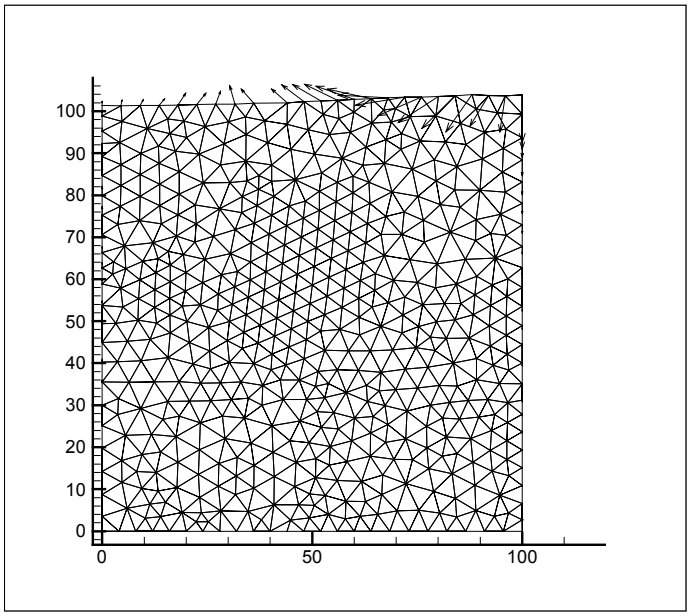

Figure 5(b): Free-surface profile at 5.5 time units.

It is observed from the simulations that the sloshing dampens quickly and the free-surface assumes a horizontal shape at steady state conditions, as per our expectations. Figures 5(a)-(b) indicate the intermediate shapes of the free-surface at various stages of sloshing. The arrows in the pictures represent the local velocity vectors.

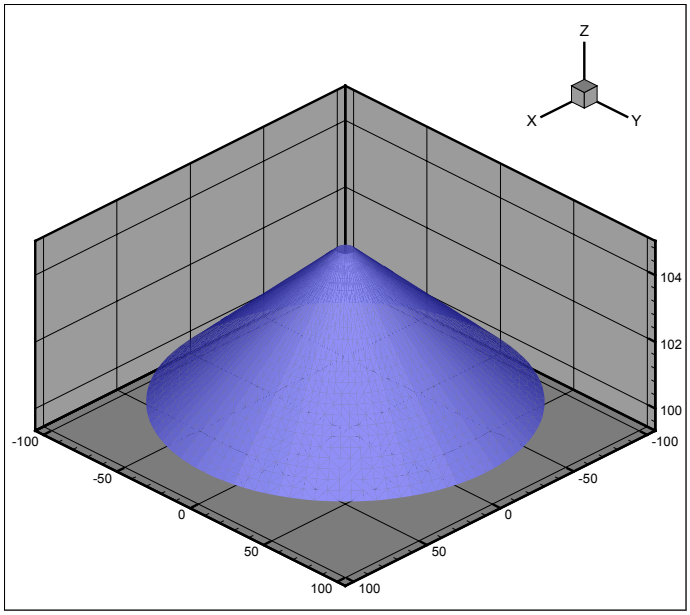

Figure 6(a): Initial shape of the free-surface.

7.2.2 Axi-symmetric sloshing of a viscous sloshing in a cylindrical container: Axi-symmetric version of the code is implemented to simulate the sloshing of a viscous liquid in a cylindrical container. Figures 6(a)-(d) present the time series of evolution of the free surface. The free-surface starts with a

conical profile as shown in in fig 6(a). The maximum Reynold's number in the problem is approximately 500.

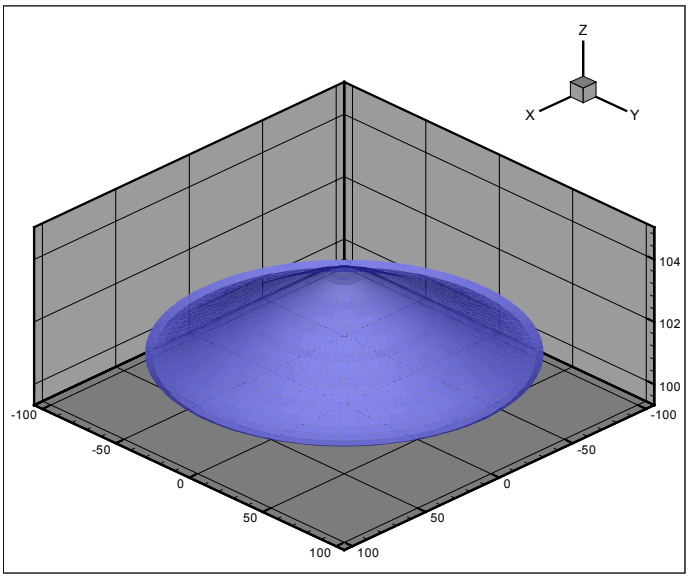

Figure 6(b): Free-surface profile at 2.83 time units.

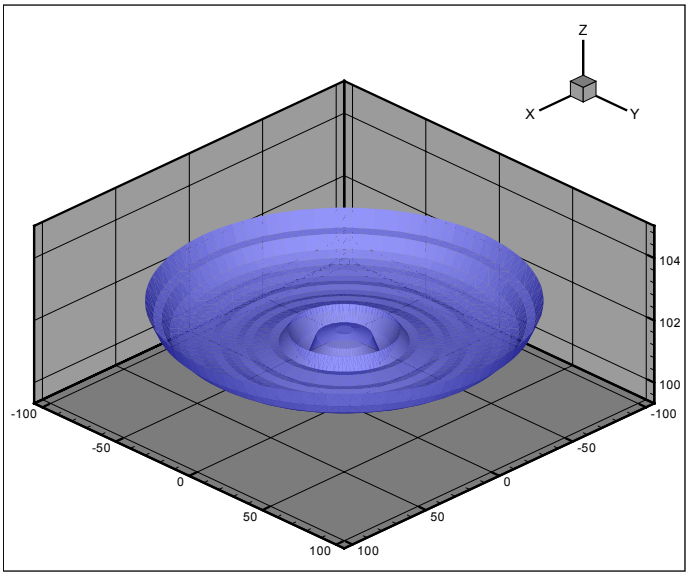

Figure 6(c): Free-surface profile at 4.25 time units.

7.2.3 Droplet impingement on a wall: The problem consists of a cylindrical droplet falling freely under gravity and colliding against a solid wall. The resulting deformation of the droplet is simulated at a Reynold's number of 220 and a Weber number of 0.4. The wall is assumed to be a no-slip wall so that the portion of the drop that comes into contact with the wall remains stationary. Figures 7 (a)-(d) depict the shape of the deforming droplet at various intermediate stages.

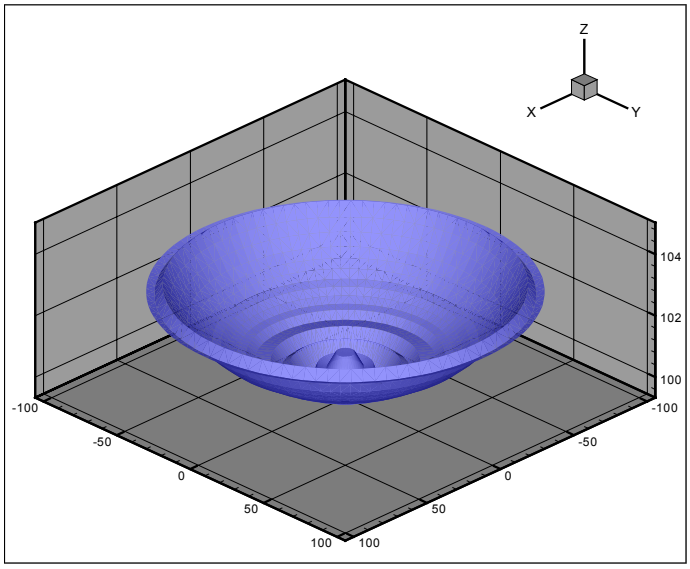

Figure 6(d): Free-surface profile at 5.67 time units.

As we see from the plots, the droplet flattens at the bottom where it hits the wall and flows radially outward, thus reducing the thickness at the axis of symmetry. The present simulation uses very low Weber and Reynold numbers, implying domination of surface tension forces and viscous forces over the viscous forces. Hence we notice that the fluid is held together as a single unit and outward flow is restricted. Also as the pictures indicate, the stream function contours shift outward on either side as the fluid sees a stagnation zone in the area where contact with the wall takes place.

Figure 7(a): Initial shape of the droplet

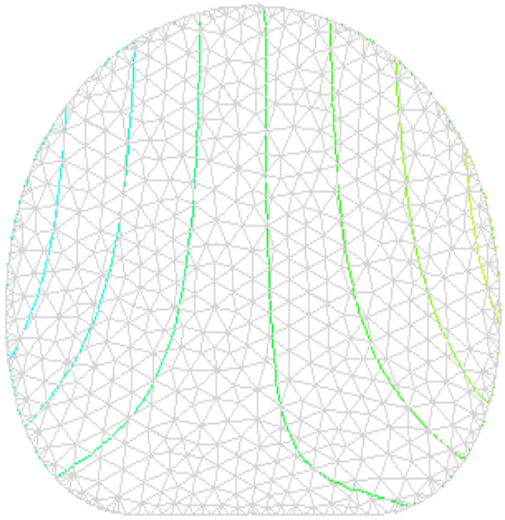

Figure 7(b) : Profile after 0.14 time units

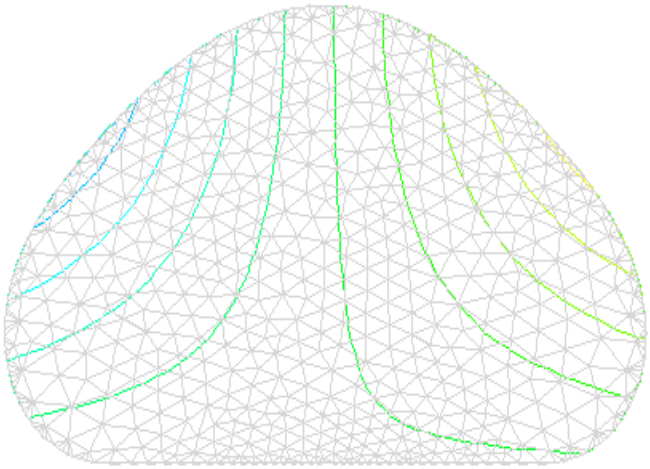

Figure 7(c): Shape of the droplet after 0.19 time units

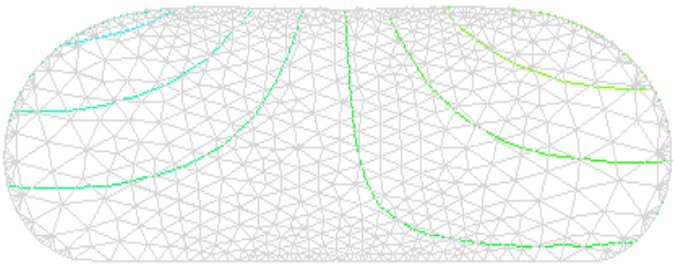

Figure 7(d): Shape of the droplet after 0.32 time units

8. Conclusions:

A new unstructured moving mesh approach is presented in this paper to solve incompressible flow problems involving free-surfaces. The code is tested and validated using the benchmark problem of irrotational sloshing in a two-dimensional rectangular tank. A few numerical examples of free-surface simulation using the present approach have also been presented.

9. References:

[1] HARLOW, F. H. & WELCH, J. E., Numerical calculations of time dependent viscous incompressible flow of fluid with a free surface, *Phys. Fluids*, **8** , 1965, p. 2182.

[2] C. A. Hall, J. S. Peterson, T. A. Porsching & F. R. Sledge, The dual variable method for finite element discretizations of Navier/Stokes equations, *Int. J. Num. Meth. Eng*., **21**, 883-898, (1985)

[3] R. A. Nicolaides, Direct discretization of planar div-curl problems, ICASE Report 89-76 (1989).

[4] R. A. Nicolaides, The covolume approach to computing incompressible flow, *Incompressible Computational Fluid Dynamics*, M. D. Gunzburger & R. A. Nicolaides, eds., Cambridge University Press, 295-234 (1993).

[5] R. A. Nicolaides and X. Wu, Covolume solutions of three-dimensional div-curl equations, ICASE Report. 95-4 (1995).

[6] Blair Perot and Xing Zhang, Reformulation of the unstructured staggered mesh method as a classic finite volume method, *Finite Volumes for Complex Applications II*, Hermes Science Publications (1999), pp. 263-270.

[7] Blair J. Perot, Conservation properties of unstructured staggered mesh schemes, *Journal of Computational Physics,* (Accepted for publication in 2000).

[8] B. Joe, Three-dimensional triangulations from local transformations, *SIAM J. Sci. Stat. Comput.*, **10**, pp.718-741(1989).

[9] F. Harlow and A. Amsden, *Fluid Dynamics, an introductory text*, Los Alamos scientific laboratory, LA-4700 (1980)